The Workflow of Ground Penetrating Radar Data Analysis Based on Maximum Energy Difference Steering

*Duy Hoang DANG[1), 2),3)], Cuong Van Anh LE[*1), 2)], Thuan Van NGUYEN[1), 2)], Long Quoc NGUYEN[4)], Nhan Thanh HUYNH[1),2)]*

[1)] University of Science, Ho Chi Minh City, Vietnam; email: lvacuong@hcmus.edu.vn
[2)] Vietnam National University Ho Chi Minh City, Vietnam
[3)] Loc Ninh Highschool, Binh Phuoc Province, Vietnam
[4)] Hanoi University of Mining and Geology, Vietnam
* Corresponding author: lvacuong@hcmus.edu.vn

http://doi.org/10.29227/IM-2023-01-25

Submission date: 20-05-2023 | Review date: 01-06-2023

Abstract

Ground Penetrating Radar is commonly used in civil engineering sectors. Underground anomalies (i.e., electric wires, water pipes or sinkholes) can be detected through representations of hyperbolae in the measured processed GPR image. Our work focuses on detecting the underground objects and understanding their metallic or nonmetallic characteristics. The max energy difference attribute is applied to illuminate their positions while phase analysis process can determine change of phase spectrum in the diffracted signals. For improving phase analysis, we applied a novel workflow combining conventional processed steps and a zooming step for preserving phase originality without disturbed by any unnecessary filters. We applied the workflow in model and real data for proving its effectiveness. Interpretation of two real datasets in Vietnam by our workflow can express existences of the artificial underground anomalies as well as their matter characteristics comparing to their surrounding environments.

Keywords: *ground penetrating radar, phase analysis, energy difference*

1. Introduction

Ground Penetrating Radar (GPR) plays a key role in detecting underground anomalies such as artificial objects or sinking holes. A conventional workflow (Le and Nguyen 2020a, Nguyen et al. 2017, Le and Nguyen 2020b, Zhao, Forte, and Pipan 2016) can convert the raw GPR data into the interpretable processed GPR data. The workflow often includes some key steps such as move-start time, background removal filter, frequency filters, gain function, velocity analysis, gain function, and migration. The processed steps can improve the ratio between signal over noise for the better recognition of underground objects, but they also can distort the original amplitudes and phases. The phase distortion will affect to analyzing metallic or unmetallic characteristics of the objects. Therefore, the original phase from the raw data needs to be kept for checking in phase or out of phase cases.

In seismic analysis, full waveform inversion is utilized to recover true acoustic impedance that answer many questions about the earth structures/ characteristics. Its input is the seismic data with preserved amplitude and phase originality (i.e., low frequency data domain) (Virieux and Operto 2009, Kumar, Ramrez, and Butt 2012). Applying the seismic spirit into GPR interpretation, we have focused on the workflow that can keep the GPR data originality and expressing the underground anomalies characteristics.

We have applied the new workflow to processing and interpreting the data. Modelling and real data are used for proving the efficiency of the workflow. The workflow focuses on two stages: (i) detecting the anomalies and (ii) analysis their phases for evaluating their matter characteristics comparing to surrounding environment.

2. Methodology

GPR data can reveal existences of different underground anomalies or ground structures by presenting their images through amplitude and phase vibrations. Raw data can be transformed into interpretable processed data by applying different filter and amplification techniques for enhancing reflection and diffraction signatures. Although diffracted hyperbolae ignited from underground objects like diffractors cannot show the true shapes of the anomalies, they can specially answer correct their positions in terms of their hyperbolae peaks (Le and Nguyen 2020a, Nguyen et al. 2017, Bitri and Grandjean 1998, Kang et al. 2019).

2.1 Conventional steps

For achieving an interpretable GPR processed data, we have applied some necessary traditional processing steps as (i) move start-time, (ii) background removal, (ii) frequency filters, and (iii) migration (Nguyen et al. 2017, Le and Nguyen 2020a, Le and Nguyen 2020b). Firstly, move start-time is so important in giving correct travel time of a real event by moving the start time of sources to zeroes. Background removal can delete background noises and frequency filters can focus on meaningful frequency band for enhancing the useful signal representation. Finally, the function of the migration step is to present the correct positions and shapes of anomalies. In our work, Kirchhoff migration is utilized (Nguyen et al. 2017, Le and Nguyen 2020a, Le and Nguyen 2020b).

For further interpretation, some GPR attribute processing steps could be applied (Fig. 1) (Nguyen et al. 2017, Le and Nguyen 2020b). For detecting anomalies, maximum energy difference can illuminate existence of anomalies and help to

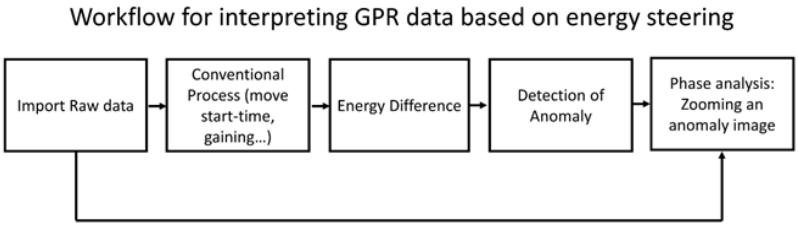

Fig. 1. The workflow of detecting metallic or unmetallic characteristics

Rys. 1. Proces wykrywania cech metalicznych lub niemetalicznych

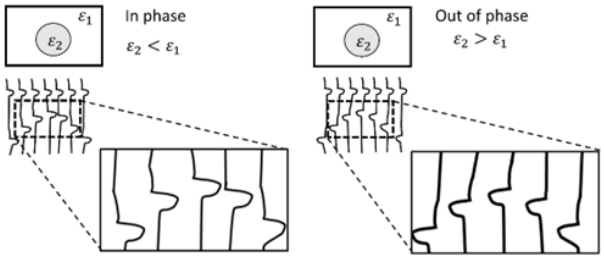

Fig. 2. In phase zooming and out of phase zooming

Rys. 2. Powiększanie w fazie i powiększanie poza fazą

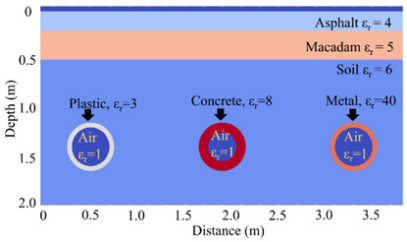

Fig. 3. Model representation

Rys. 3. Reprezentacja modelu

evaluate electromagnetic wave velocity within underground media (Nguyen et al. 2017).

Phase analysis aims to detect metal or unmetallic characteristics of an object. In phase or out of phase (Kang et al. 2019) come from phase variation of wave phase when the wave reflects from bigger to smaller electric permittivity zones and vice versa, respectively (Fig. 2).

2.2 The maximum energy difference steering workflow

In geophysical method areas like seismic and GPR, color is one kind of their special attributes (Chopra and Marfurt 2007, Le et al. 2016, Le, Harris, and Pethick 2019, Kang et al. 2020). In Kang et al. (2019) 's work, removal of the first wave can enhance the GPR data interpretation in defining in phase or out of phase cases. Our suggested workflow consists of two stages for examining an underground anomaly from the GPR data measurement: (i) Defining positions and true images of underground anomalies and (ii) analyzing phase shapes for determining the contrast of two media in which metallic or unmetallic matters are decided. Their positions can be located through their hyperbolae or visible strong GPR attributes after processing the raw data (Kang et al. 2019, Kang et al. 2020, Le and Nguyen 2020a, Le and Nguyen 2020b). Moreover, the processed phase can reveal the variation of environmental electric permittivity.

For preserving the phase information, only the move start-time step is applied. It does not harm the deeper original signals like other gain functions or many amplitude-distorted filters steps. The key thing is that recorded amplitude of first direct GPR wave is much stronger than any GPR waves travel down and bounce back from ground reflectors or diffractors. Therefore, a zooming image which shows only anomaly signals is much clearer when it does not include the first direct wave.

The conventional processing workflow is effective in detecting positions of anomalies (see Fig. 1) (Dang, Le, and Kieu 2020, Nguyen et al. 2017, Le and Nguyen 2020b). Firstly, the raw input data is processed through many conventional steps as move start-time, background filter, frequency filter, dewow, and gain function. Second, the processed are input for the maximum energy difference approach for object position estimation and velocity valuation (Nguyen et al. 2017). Third, positions and true shape of underground anomalies are achieved from Kirchhoff migration with the suitable velocity. Finally, hyperbolae phase signatures which are extracted from the processed and the first step (only move start-time) data are compared with the first direct wavelet for deciding in-phase or out of phase cases in explaining the characteristics of anomaly materials (Fig. 2).

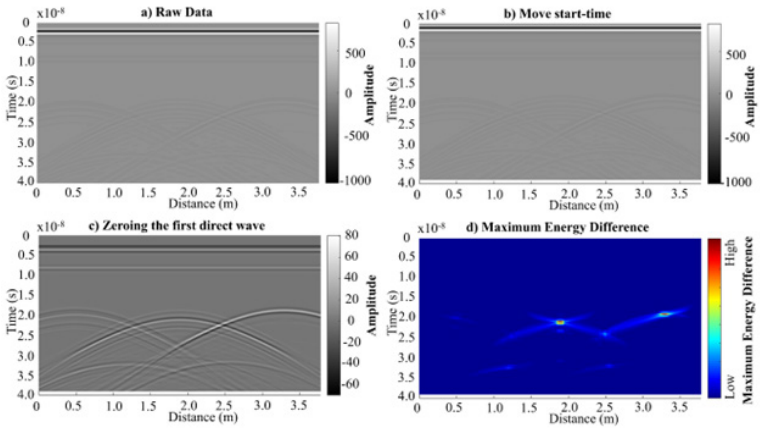

Fig. 4. Synthetic data and its processed data: a) Raw data is simulated from the model which show strongest amplitude of the first direct wave and weak hyperbolae signals. b) Move start time step is applied to raw data for representing correct wave travel time. c) The processed step is zeroing the first direct wave for illuminating the real signals of three circular objects. d) Maximum energy difference section which is computed can reveal strong values in time nearly 2.10^{-8} (s) or 20 ns for explaining their locations

Rys. 4. Dane syntetyczne i dane przetworzone: a) Surowe dane są symulowane z modelu, który pokazuje najsilniejszą amplitudę pierwszej fali bezpośredniej i słabe sygnały hiperboli. b) Krok czasu rozpoczęcia ruchu jest stosowany do surowych danych w celu przedstawienia prawidłowego czasu podróży fali. c) Przetworzony krok zeruje pierwszą falę bezpośrednią w celu oświetlenia rzeczywistych sygnałów trzech okrągłych obiektów. d) Maksymalna sekcja różnicy energii, która jest obliczana, może ujawnić silne wartości w czasie prawie $2{,}10^{-8}$ (s) lub 20 ns w celu wyjaśnienia ich lokalizacji

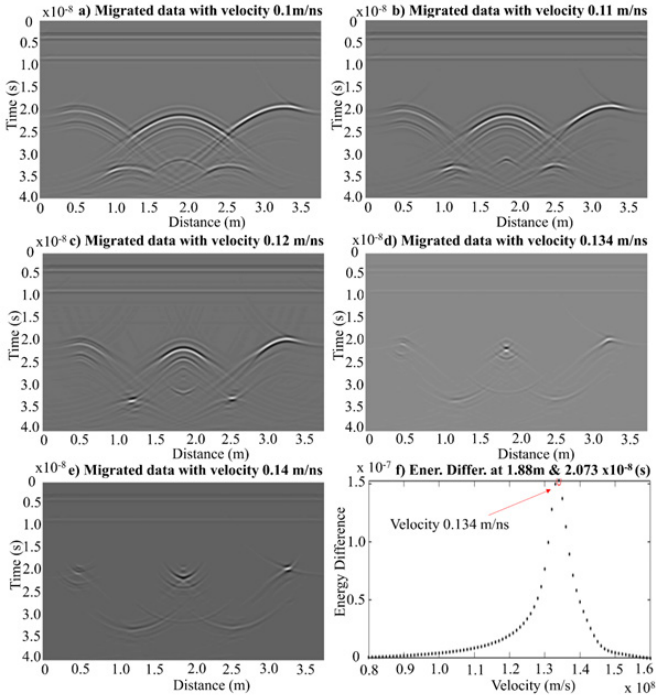

Fig. 5. Migration of Synthetic GPR data with different velocities and representation of energy difference versus velocity in the position 1.88 m and 2.073 x 10^{-8} (s)

Rys. 5. Migracja syntetycznych danych GPR z różnymi prędkościami i przedstawienie różnicy energii w funkcji prędkości w pozycji 1,88 m i 2,073 x 10^{-8} (s)

3. Results and Discussion

We applied our workflow for detecting the matter characteristics in the modelling data and real data.

3.1 Modelling data

We have used GPRMAX (Warren, Giannopoulos, and Giannakis 2016) for running synthetic data from the prior model (Fig. 3). The center frequency is 700 MHz. The model has three horizontal layers and three circular blocks (Fig.3). The three layers are asphalt, macadam, and clay with relative electric permittivity values as 4, 5, and 6, respectively. Besides, the three circular blocks which contain air inside are made up plastics, concrete, and metal with relative electric permittivity values as 3, 8, 40, respectively. Their outside radius values are 0.25 m while their inside radiuses are assigned 0.20 m, 0.15 m, and 0.20m for plastics, concrete, and metal, respectively.

In Fig. 4, the color representation is dependent on the minimum and maximum values of the direct waves. The extremes can prevent visualization of other deeper useful events such as three hyperbolae resulting from the three circular objects (Figs. 4a and 4b). This disadvantage inspires us to apply the removal technique of first direct wavelet. Therefore,

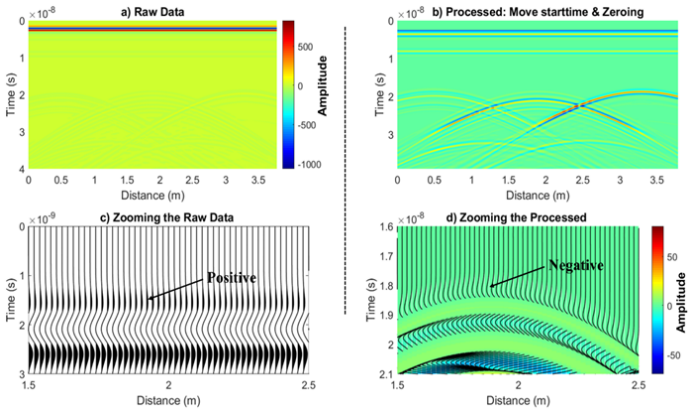

Fig. 6. Zooming image for analyzing phase

Rys. 6. Powiększenie obrazu do analizy fazy

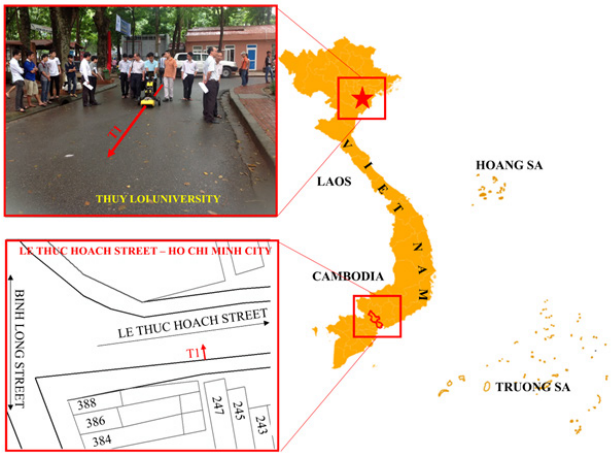

Fig. 7. Survey map for two locations (Ha Noi and Ho Chi Minh City) in Vietnam

Rys. 7. Mapa badania dla dwóch lokalizacji (Ha Noi i Ho Chi Minh City) w Wietnamie

zeroing the first direct wave is applied to this synthetic data (Fig. 4c).

For evaluation of wave propagation velocity, we tested many migrated sections (Fig. 5) with different velocities varying around the velocity picked by analysis of 1D maximum energy difference curve (Fig. 5f). Over-, focused and under- migration phenomena are easily seen in the sections with bigger values, correct value, and lower velocity values, respectively. The velocity 0.12 m/ns (meter per nano second) is chosen for calculating the circular anomalies 's depths for providing better depth value than the one 0.134 m/ns. The value 0.134 m/ns has an tendency gives the bigger depth because the Kirchhoff migration tries to compress the big circular shapes of the big anomalies (Le and Nguyen 2020a).

Besides, the processed zeroing data, migrated, and maximum energy difference sections can shed light on locations of the three circular anomalies in time nearly 2.10-8 (s).

The first and third objects at locations 0.56 m and 3.36 m can represent the phase types as in-phase and out of phase, respectively. However, the second object at x=1.88m needs more works to clarify its phase characteristics because of weak first break amplitudes. Therefore, Fig. 6 expresses two zooming images of the area containing the second object. It looks like that its first wavelet (Fig. 6c) is negative which is contrary to the positive wavelet of the first direct wave (Fig. 6d). Therefore, it is out of phase case compatible with the electric permittivity values of the second object and the surrounding background. Notice that the zooming image extracted from the zeroing first direct data (Fig. 4c) can show the hyperbolae so well.

3.2 Real data

Field data 1:

The electromagnetic method survey was conducted in Thuy Loi university, Ha Noi, Vietnam. We have used the GPR equipment branded IDS Duo Detector, 700 MHz, made in Italy (Fig. 7). The processed and maximum energy difference are computed from the raw data shown in Fig. 8. We can detect the position of a hyperbola = 3.424m and t=1.375x 10-8 (s) in the two processed attribute images (Figs. 8c and d). To analyze the position of artificial object at x= 3.424m and t=1.375x 10-8 (s), many migrated sections are analyzed (Fig. 9). The object is interpreted as the drainage pipe from the prior information. We can achieve the velocity of wave propagation at 0.074 m/ns to give its depth at 0.41m with the first wavelet time 1.1x 10-8 (s).

For phase analysis in zooming image (Fig. 10), first wave direct wave (Fig. 8a) and the first wavelet of its hyperbola are compared. In zooming images of Fig. 10, the trough shape (i.e., negative values) are seen in the processed and raw data.

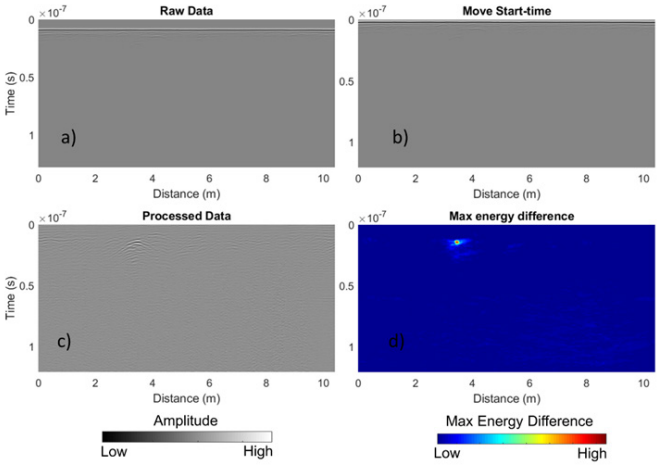

Fig. 8. The raw, move Start-time, processed data and its maximum energy difference attribute

Rys. 8. Nieprzetworzone, przesunięte w czasie, przetworzone dane i ich atrybut maksymalnej różnicy energii

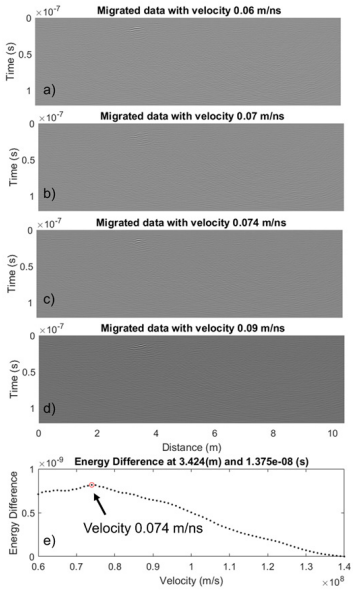

Fig. 9. Migration sections with different velocities and 1D Maximum energy difference curve versus velocities

Rys. 9. Odcinki migracji z różnymi prędkościami i krzywa maksymalnej różnicy energii 1D w funkcji prędkości

Notice that the first wavelet of the direct first wave is positive in the real data (Fig. 8a). This can explain that the electric permittivity of the object is more than the electric permittivity of the surrounding environment. In prior information seen in Fig. 7, the drainage pipe is made of concrete.

Field data 2:

We also conducted the GPR equipment as IDS Duo Detector, 700 MHz in Le Thuc Hoach street, Tan Phu District, Ho Chi Minh City, Vietnam. The raw data is processed the same workflow mentioned in the methodology (Fig. 11) (see Section 2.2). Its conventionally processed data shown in Fig. 11c and its maximum energy difference section in Fig. 11d can express location of one object. The object is known as a metal water supplying water. Its position has x=1.615 m and 2.3 x 10-8 (s). For computing its depth, we tested several migrated sections in Fig. 12. Under and over migration effects can be seen in Figs. 12a and b, and Fig. 12d, respectively. The chosen velocity, 0.087 m/ns, which is extracted from the 1D maximum energy difference curve (Fig. 12f), can estimate its depth at 0.94m with its first break 2.1 x 10-8 (s).

In the phase analysis stage, we represent two types of processed data and raw data in for zooming images (Fig. 13). Notice that the raw data does not receive any amplitude filter except move start-time step so it does keep its true amplitude. Negative effect is strongly seen in all the four zooming images. The out of phase case can expresses that the electromagnetic wave bounced at the anomaly having the electric permittivity bigger than the surrounding environment. The object interpretation is suitable the prior information that the supplying water pipe is metallic.

4. Conclusion

We have applied our workflow to investigate positions and characteristics of underground anomalies. The workflow focuses on detection of positions using maximum energy difference approach and phase analysis using in phase and out of phase cases. Besides, migration technique helps to estimate

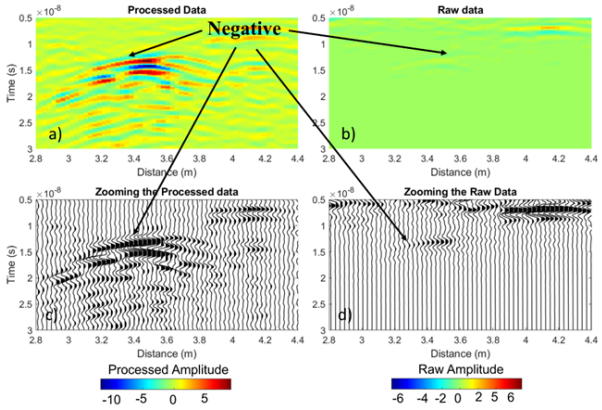

Fig. 10. zooming image for analyzing phase

Rys. 10. Powiększanie obrazu do analizy fazy

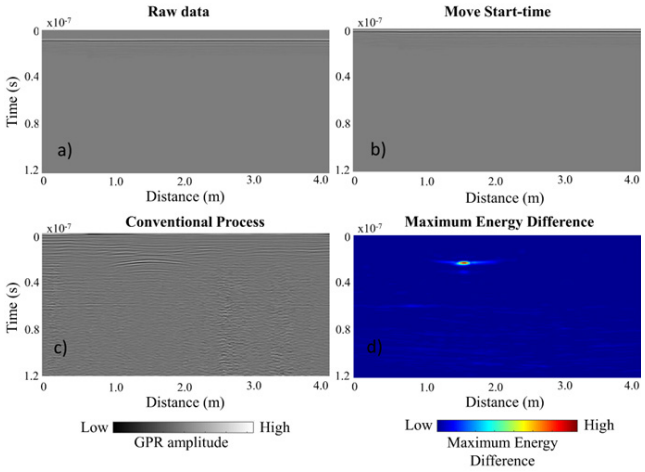

Fig. 11. The raw, Move Start-time, processed data and its maximum energy difference attribute in LeThuc Hoach street, Tan Phu district, Ho Chi Minh City, Vietnam

Rys. 11. Przetworzone dane surowe, czas rozpoczęcia ruchu i atrybut maksymalnej różnicy energii na ulicy LeThuc Hoach, dzielnica Tan Phu, miasto Ho Chi Minh, Wietnam

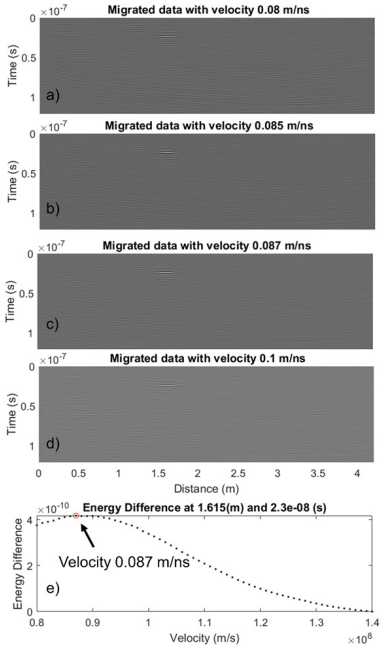

Fig. 12. Migration sections with different velocities and 1D Maximum energy difference curve versus velocities in Le Thuc Hoach street, Tan Phu district, Ho Chi Minh city, Vietnam

Rys. 12. Odcinki migracyjne o różnych prędkościach i krzywa maksymalnej różnicy energii 1D w zależności od prędkości na ulicy Le Thuc Hoach, dzielnica Tan Phu, miasto Ho Chi Minh, Wietnam

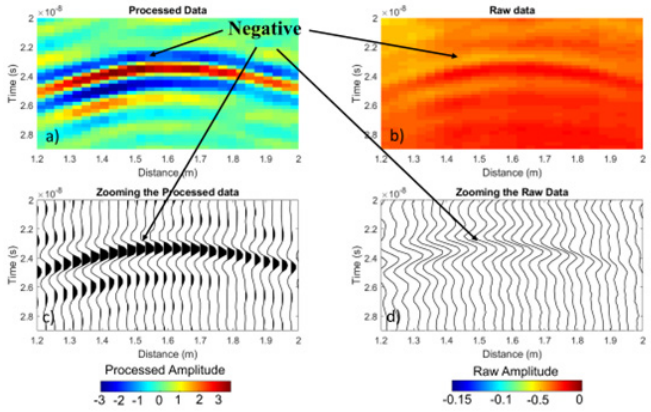

Fig. 13. Zooming image for analyzing phase of the processed and raw data in the interest zone containing a hyperbola

Rys. 13. Powiększanie obrazu do analizy fazy przetworzonych i nieprzetworzonych danych w strefie zainteresowania zawierającej hiperbolę

depths of the anomalies. For enhancing phase interpretation, we combine two zooming images of the raw and processed data for checking in-phase or out of phase cases in one modelling data and two real data. The originality of the raw data which can be seen in zooming image can be kept for checking the phase effects along with its processed data.

Acknowledgments

This research is funded by University of Science, VNUH-CM under grant number T2022-53.

Conflicts of Interest

The authors declare no conflict of interest.

Author Contribution

DHD run data modelling and data processing. CVAL wrote processing/ analysis Matlab codes for the GPR approach and interpreted GPR data. TVN measured real GPR data. LQN and NTH support data processing and manuscript writing. CVAL mainly write the manuscript.

Literatura – References

1. Bitri, A., and G. Grandjean. 1998, Frequency–wavenumber modelling and migration of 2D GPR data in moderately heterogeneous dispersive media. Geophysical Prospecting, 46, no. 3,287-301.
2. Chopra, S., and K. J. Marfurt. 2007, Seismic attributes for prospect identification and reservoir characteriztion. Edited by Stephen J. Hill, SEG Geophysical Development Series No. 11: Tulsa, Okla. (8801 South Yale St., Tulsa OK 74137-3175) : Society of Exploration Geophysicists.
3. Dang, D. H., C. V. A. Le, and T. D. Kieu. 2020, Ground Penetrating Radar attribute for analyzing underground anomaly. Paper read at EAGE 3rd Asia Pacific Meeting on Near Surface Geoscience & Engineering.
4. Kang, M.-S., N. Kim, S. B. Im, J.-J. Lee, and Y.-K. An. 2019, 3D GPR Image-based UcNet for Enhancing Underground Cavity Detectability. Remote Sensing, 11, no. 21,2545.
5. Kang, M.-S., N. Kim, J. J. Lee, and Y.-K. An. 2020, Deep learning-based automated underground cavity detection using three-dimensional ground penetrating radar. Structural Health Monitoring, 19, no. 1,173-185.
6. Kumar, J., A. C. Ramrez, and S. Butt. 2012, Preparing Data for Full Waveform Inversion: A Workflow for Free-surface Multiple Attenuation. Paper read at 74th EAGE Conference and Exhibition-Workshops.
7. Le, C. V. A., B. D. Harris, and A. M. Pethick. 2019, New perspectives on Solid Earth Geology from Seismic Texture to Cooperative Inversion. Scientific Reports, 9, no. 1,14737. doi: 10.1038/s41598-019-50109-z.
8. Le, C. V. A., B. D. Harris, A. M. Pethick, E. M. Takam Takougang, and B. Howe. 2016, Semiautomatic and Automatic Cooperative Inversion of Seismic and Magnetotelluric Data. Surveys in Geophysics, 37, no. 5,845-896. doi: 10.1007/s10712-016-9377-z.
9. Le, C. V. A., and T. V. Nguyen. 2020a, Detection of Underground Anomalies Using Analysis of Ground Penetrating Radar Attribute. Inżynieria Mineralna – Journal of the Polish Mineral Engineering Society, 1,23-34.
10. Le, C. V. A., and T. V. Nguyen. 2020b, Ground penetrating radar attributes analysis for detecting underground artificial structures in urban areas, Vietnam. Lowland Technology International, 22, no. 2,249-257.
11. Nguyen, T. V., C. V. A. Le, V. T. Nguyen, T. H. Dang, T. M. Vo, and L. N. L. Vo. 2017, Energy Analysis in Semiautomatic and Automatic Velocity Estimation for Ground Penetrating Radar Data in Urban Areas: Case Study in Ho Chi Minh City, Vietnam, International Conference on Geo-Spatial Technologies and Earth resources: Springer.
12. Virieux, J., and S. Operto. 2009, An overview of full-waveform inversion in exploration geophysics. Geophysics, 74, no. 6,WCC127–WCC152.
13. Warren, C., A. Giannopoulos, and I. Giannakis. 2016, gprMax: Open source software to simulate electromagnetic wave propagation for Ground Penetrating Radar. Computer Physics Communications, 209,163-170.
14. Zhao, W., E. Forte, and M. Pipan. 2016, Texture attribute analysis of GPR data for archaeological prospection. Pure and Applied Geophysics, 173, no. 8,2737-2751.

Przebieg pracy z danymi radarowymi penetrującymi ziemię. Analiza oparta na sterowaniu maksymalną różnicą energii

Ground Penetrating Radar jest powszechnie stosowany w inżynierii lądowej i wodnej. Podziemne anomalie (np. przewody elektryczne, rury wodociągowe lub zapadliska) można wykryć za pomocą reprezentacji hiperbol w zmierzonym przetworzonym obrazie GPR. Nasza praca koncentruje się na wykrywaniu podziemnych obiektów i zrozumieniu ich metalicznych lub niemetalicznych wła-ściwości. Atrybut maksymalnej różnicy energii jest stosowany do oświetlania ich pozycji, podczas gdy proces analizy fazowej może określić zmianę widma fazowego w dyfrakcyjnych sygnałach. Aby usprawnić analizę fazową, zastosowaliśmy nowatorski przepływ pracy łączący konwencjonalne kroki przetwarzania i krok powiększania w celu zachowania oryginalności fazy bez zakłócania przez niepotrzebne filtry. Zastosowaliśmy przepływ pracy w modelu i rzeczywistych danych, aby udowodnić jego skuteczność. Interpretacja dwóch rzeczywistych zbiorów danych w Wietnamie za pomocą naszego przepływu pracy może wyrazić istnienie sztucznych anomalii podziemnych, a także ich charakterystykę materii w porównaniu z otaczającym je środowiskiem.

Słowa kluczowe: *radar penetrujący podłoże, analiza fazowa, różnica energii*